Supporting Information

Poly(viologen halide)s: Both Cationic Main-Chain and Counter Anions are Active for High-Performance Organic Cathodes

Zhaolei Wang,[a] *An Duan*,[b] *Weize Jin*,[a] *Xiaoyu Huang*,[a,b,*] *Yongjun Li*[a,*]

[a] Key Laboratory of Synthetic and Self-Assembly Chemistry for Organic Functional Molecules, Center for Excellence in Molecular Synthesis, Shanghai Institute of Organic Chemistry, University of Chinese Academy of Sciences, Chinese Academy of Sciences, 345 Lingling Road, Shanghai 200032, People's Republic of China.

[b] School of Physical Science & Technology, ShanghaiTech University, 100 Haike Road, Shanghai 201210, People's Republic of China.

* To whom correspondence should be addressed, E-mail: liyongjun78@sioc.ac.cn (Y. Li), xyhuang@sioc.ac.cn (X. Huang).

Experimental Section

1. Materials synthesis and characterizations

4,4-Biprydine (98%), bromoethane (99%), 4-vinybenzyl chlorine (99%), $K_2S_2O_8$ (98%), NH_4PF_6 (98%), tetrabutylammonium bromide (98%), tetrabutylammonium iodide (98%) were purchased from TCI and used as received. All the solvents were purchased from Sinopharm and used as received without further purification.

All NMR analyses were performed on JEOL JNM-ECZ400 spectrometer (400 MHz) in D_2O and CD_3CN, tetramethylsilane was used as an internal standard; Fourier transform infrared spectroscopy (FT-IR) was carried out with a Nicolet AVATAR-360 FT-IR spectrophotometer with a 4 cm^{-1} resolution; UV/vis absorption spectra were recorded on a Hitachi U-2910 spectrophotometer; Scanning electron microscopy (SEM) were obtained on Nova NanoSEM 450. X-ray photoelectron spectroscopy (XPS) were collected with a Thermo Fisher Scientific ESCALAB 250Xi X-ray Photoelectron Spectrometer. Raman spectra were carried out on a Thermo Scientific-DXR Raman Microscope with an excitation laser of 633 nm. Multiangle laser light scattering (MALLS) measurements were performed by the Wyatt Technology DAWN HELEOS 18 angle light scattering detector using Ga-As laser (661 nm). The refractive index increments (dn/dc) of PVBVEtBrCl in aqueous solution were determined at 25 °C by an Optilab Rex interferometeric refractometer (Wyatt Technology) at wavelength of 658 nm, and the concentrations of PVBVEtBrCl determined in aqueous solution for Zimm plot were 1.22, 0.82, 0.57, 0.34 mg/mL.

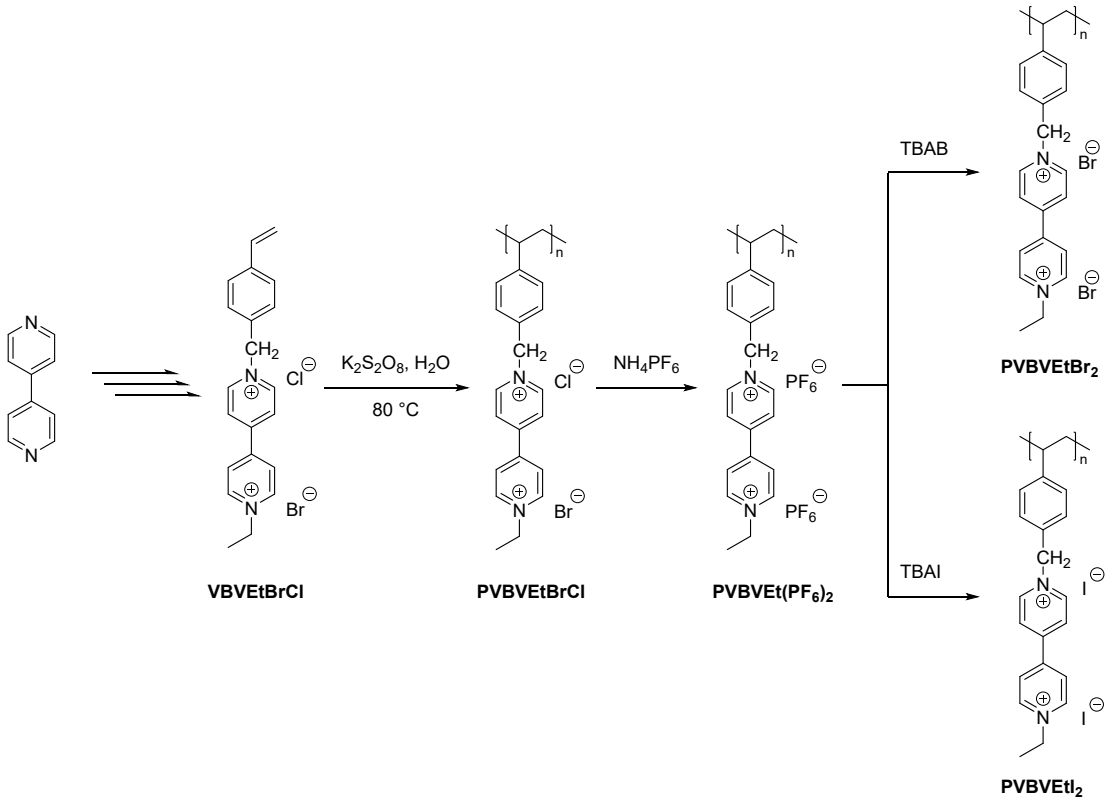

Scheme S1. Synthesis of PVBVEtX_2, X=PF_6, Br, I.

1.1 Synthesis of EtVBr

4,4-Biprydine (6.24 g, 40 mmol) and bromoethane (751 μL, 10 mmol) were dissolved in acetonitrile (40 mL) and refluxed for 24 h. After cooling to room temperature, the solvent was removed under vacuum, and the solid product was dissolved in DMF at 100 °C. The reaction mixture was filtrated and washed with hot DMF for three times. The filtrate was precipitated in ether, and dried under vacuum to afford product with a yield of 67%. ^{1}H NMR (400 MHz, D_2O): δ (ppm): 8.81 (d, J = 6.5 Hz, 2H), 8.59 (d, J = 6.2 Hz, 2H), 8.23 (d, J = 6.3 Hz, 2H), 7.73 (d, J = 5.9 Hz, 2H), 4.54 (q, J = 7.3 Hz, 2H), 1.51 (t, J = 7.5 Hz, 3H). ^{13}C NMR (101 MHz, D_2O): δ (ppm): 149.93, 144.49, 142.62, 126.01, 122.46, 57.06, 15.62.

1.2 Synthesis of VBVEtBrCl

The mixed solution of 4-vinybenzyl chlorine (2 mL, 0.014 mol) and EtVBr (0.96 g, 0.005 mol) in anhydrous acetonitrile (25 mL) was stirred for 24 h at 80 °C in the oil bath. The resulting solution was filtrated and then the yellow precipitate was purified with anhydrous diethyl ether and dried in vacuum to give VBVEtBrCl (1.36 g, 90%). ^{1}H NMR (400 MHz, D_2O): δ (ppm): 8.97 (dd, *J* = 13.1, 6.6 Hz, 4H), 8.35 (t, *J* = 5.6 Hz, 4H), 7.43 (d, *J* = 7.8 Hz, 2H), 7.33 (d, *J* = 8.0 Hz, 2H), 6.64 (dd, *J* = 17.8, 11.0 Hz, 1H), 5.78-5.69 (m, 3H), 5.21 (d, *J* = 10.8 Hz, 1H), 4.58 (q, *J* = 7.4 Hz, 2H), 1.52 (t, *J* = 7.4 Hz, 3H). ^{13}C NMR (101 MHz, D_2O): δ (ppm): 150.47, 145.45, 139.16, 135.71, 131.59, 129.70, 127.21, 127.07, 126.98, 115.91, 64.49, 57.68, 15.59.

Supporting Figures

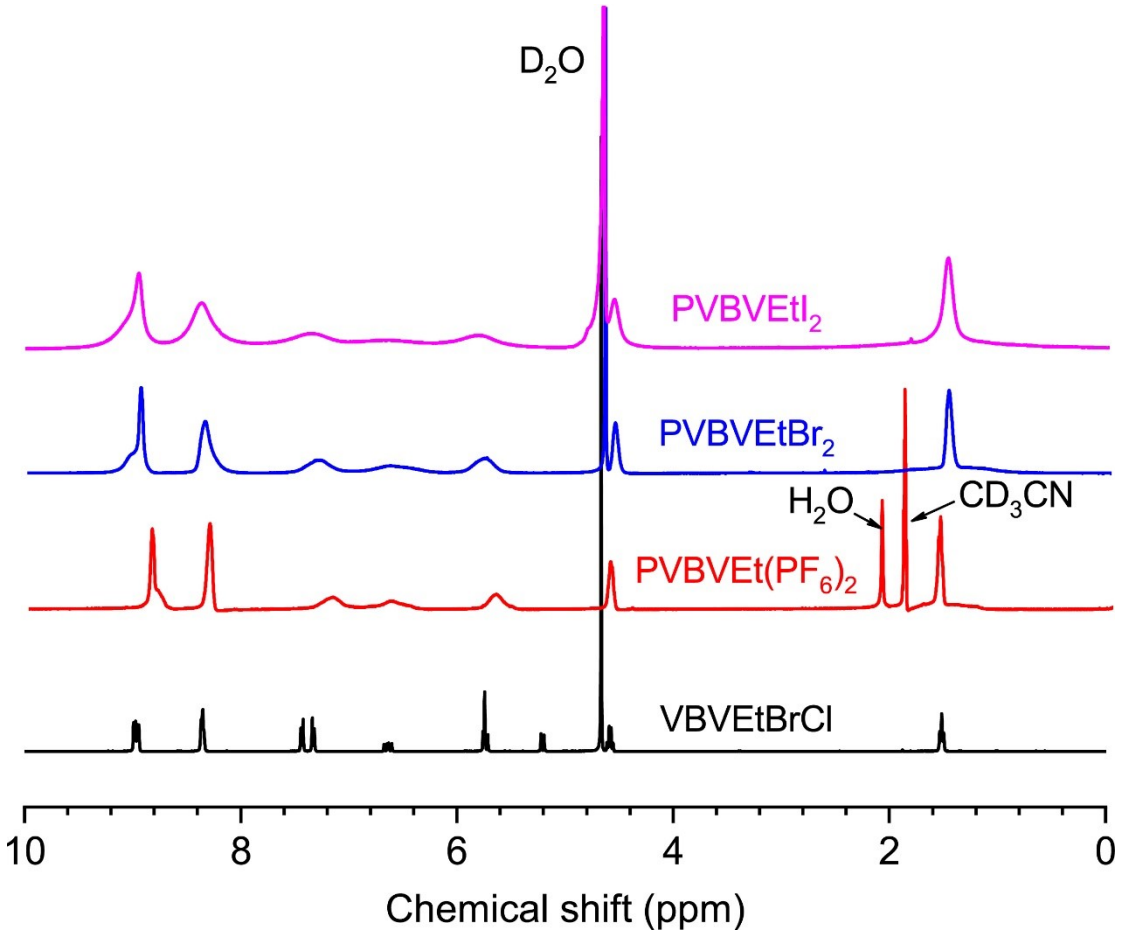

Figure S1. ^{1}H NMR spectra of the monomer VBVEtBrCl and polymers PVBVEt$(PF_6)_2$, PVBVEtBr_2 and PVBVEtI_2.

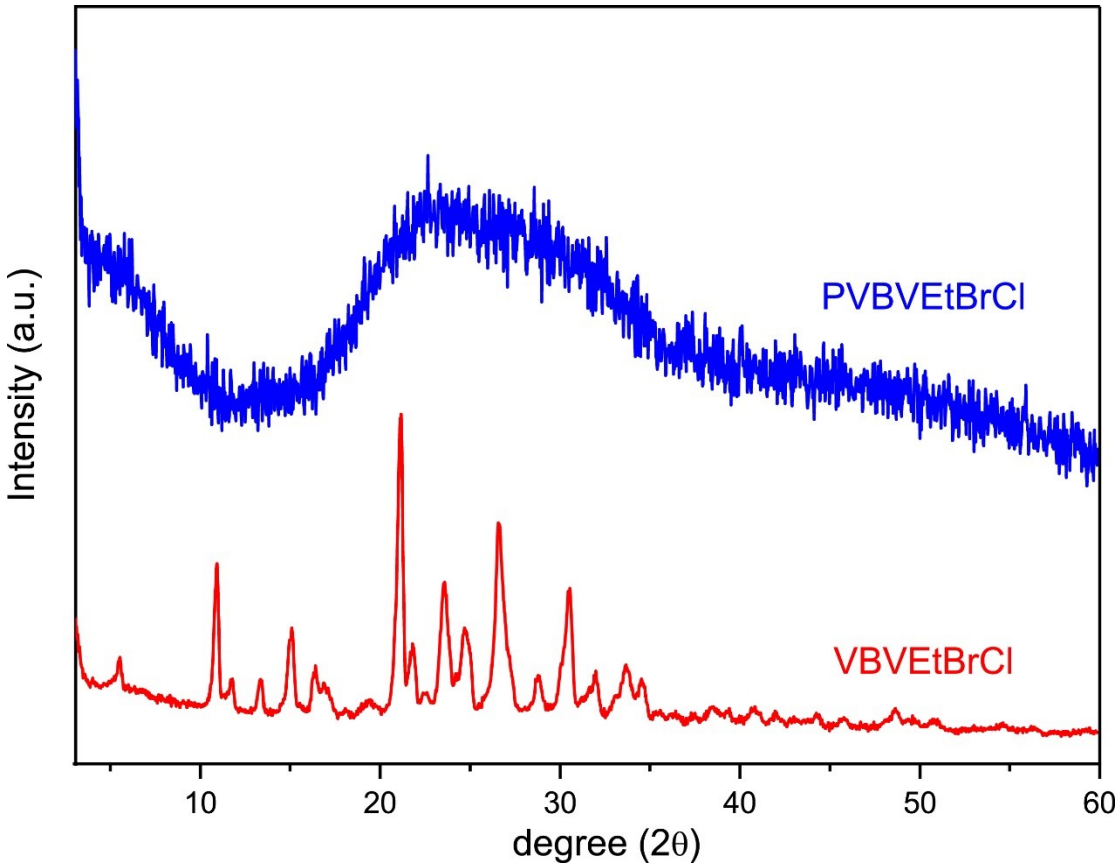

Figure S2. XRD patterns of monomer VBVEtBrCl and polymer PVBVEtBrCl.

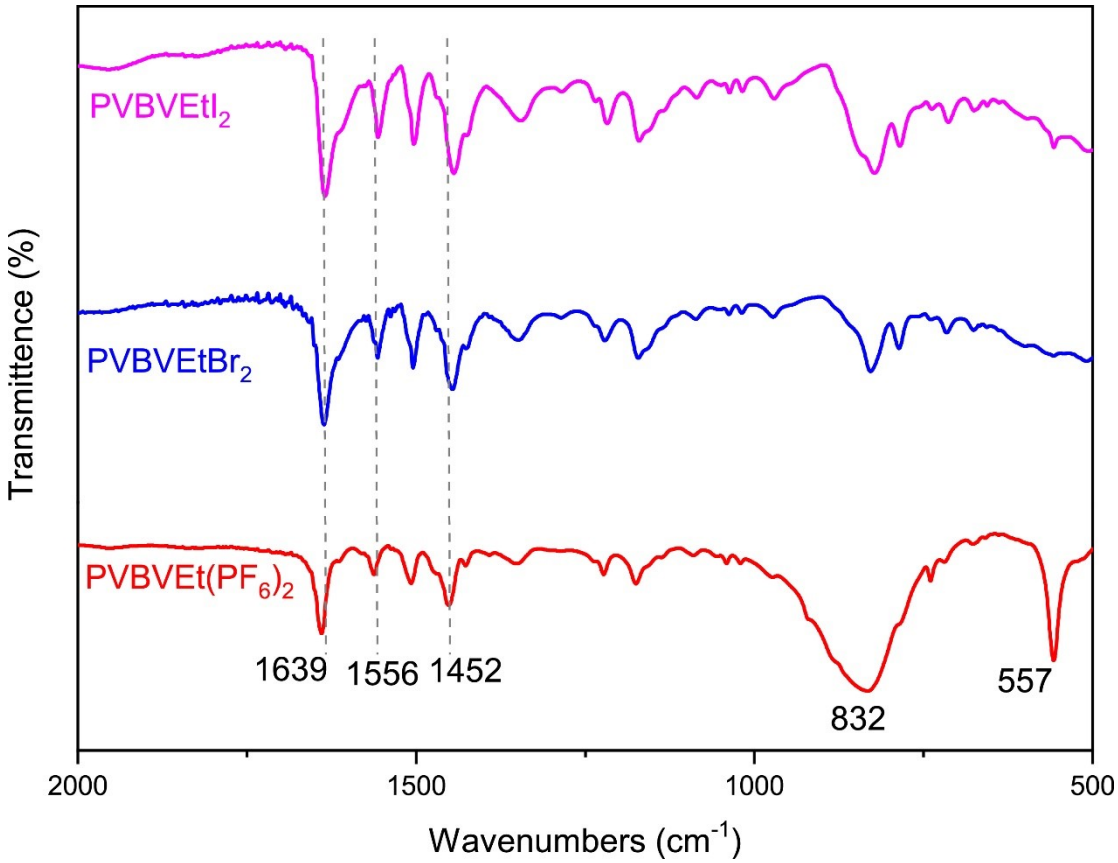

Figure S3. FT-IR spectrum of PVBVEtX_2, X=PF_6, Br, I.

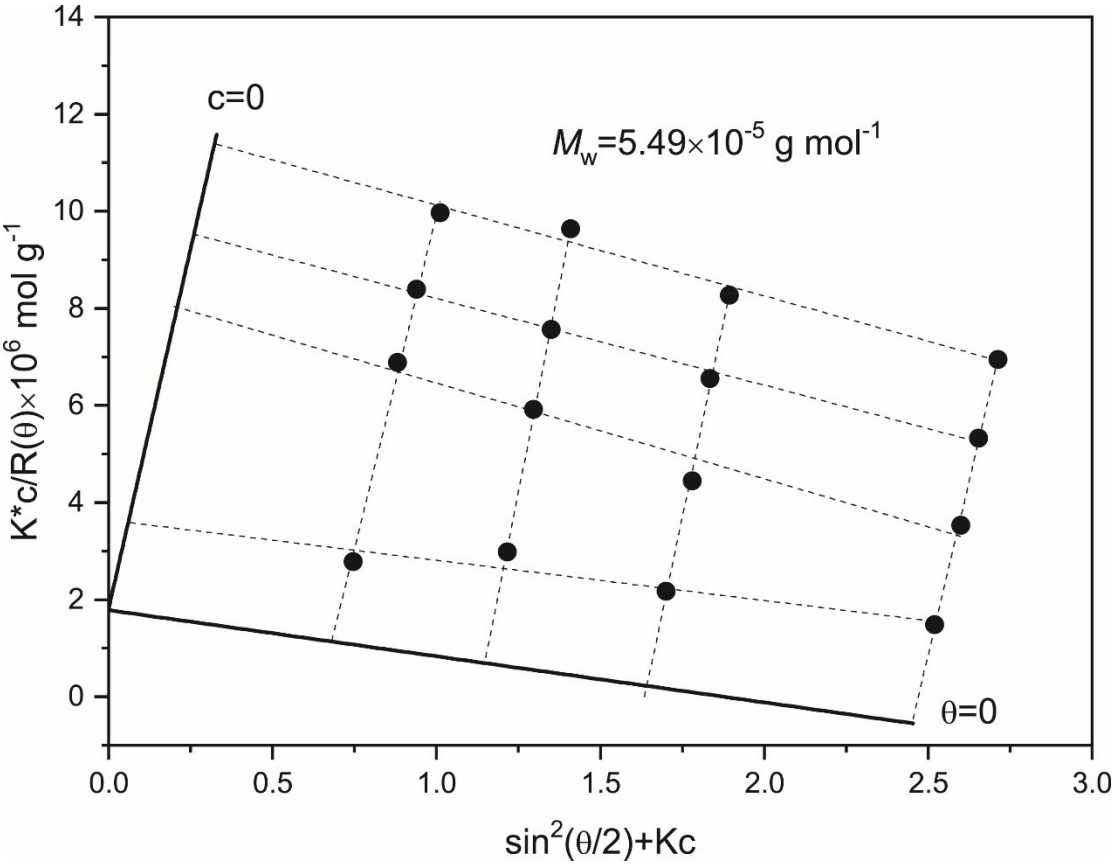

Figure S4. Typic Zimm plot for PVBVEtBrCl in water.

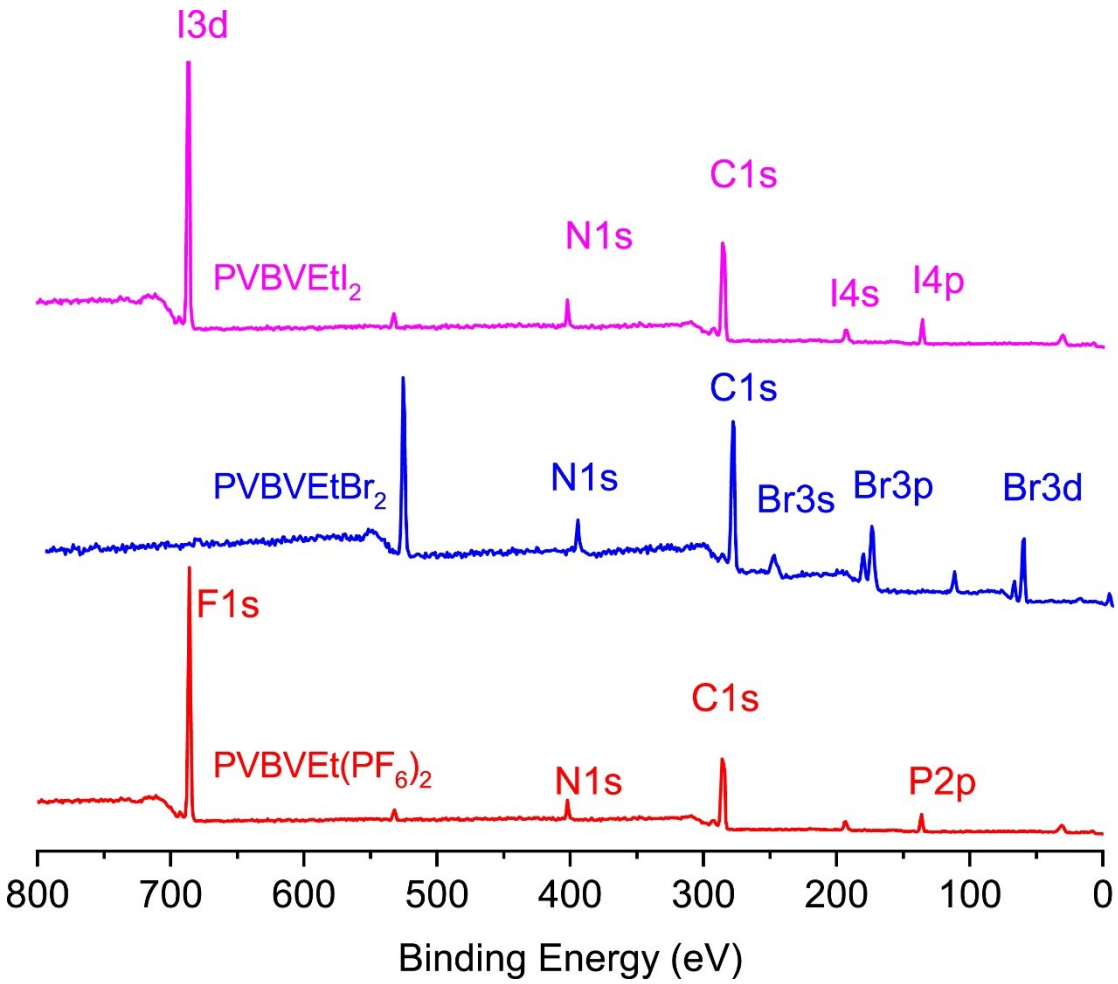

Figure S5. XPS spectra of $PVBVEt(PF_6)_2$, $PVBVEtBr_2$ and $PVBVEtI_2$ powder.

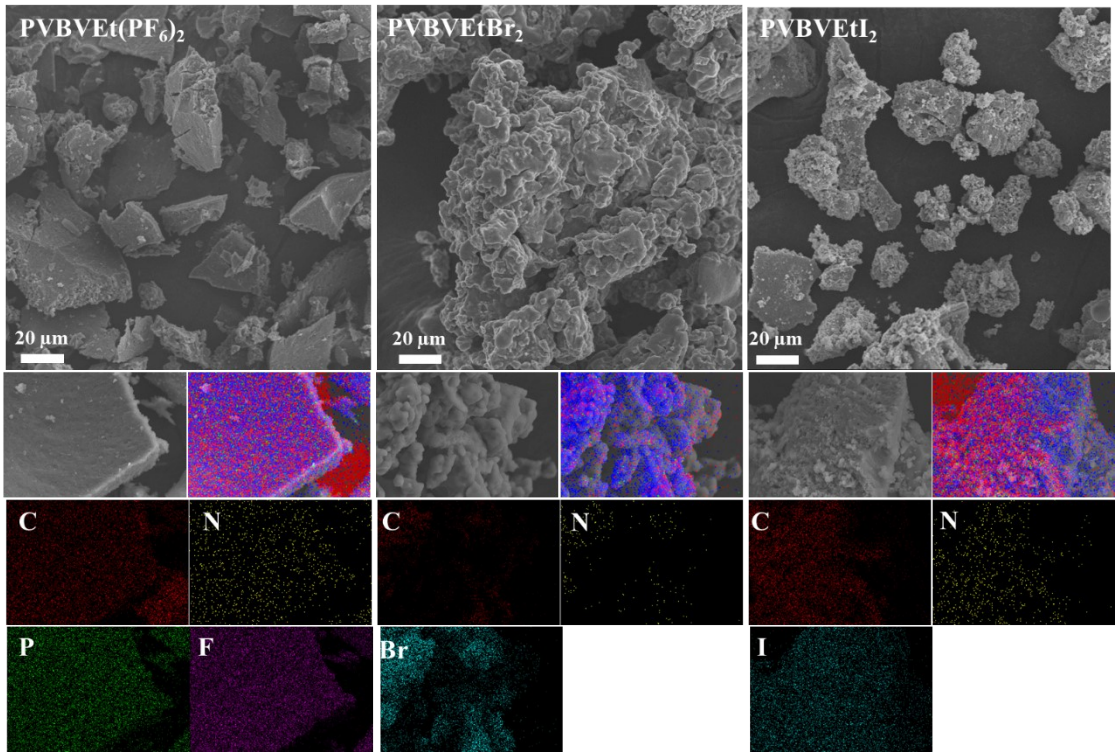

Figure S6. SEM images and corresponding elemental mapping images of $PVBVEt(PF_6)_2$, $PVBVEtBr_2$ and $PVBVEI_2$ powders.

Figure S1 shows the ^1H NMR spectra of monomer VBVEtBrCl and polymers $PVBVEtX_2$, (X = PF_6^-, Br^- and I^-). After polymerization, the signals of vinyl at 5.20, 5.71 and 6.60~6.67 ppm are disappeared, and two new broad signals at around 1.59 ppm are appeared, which corresponding to the protons of the polymer main chain. The signals of benzyl protons are up-field shifted from 7.33 to 6.52 ppm. These results all indicated the successful polymerization of monomer VBVEtBrCl. As shown in XRD patterns (Figure S2), only two broad peaks were collected in PVBVEtBrCl, indicating the conversion of VBVEtBrCl monomer into polymers. Figure S3 shows FT-IR spectra of $PVBVEtX_2$. The bands at 1639 cm^{-1} are the characteristic peaks of C-N^+, and the peaks at 1556 cm^{-1} assigned to C=C and C=N from viologen and the peaks at 1452 cm^{-1} attributed to C=C bonds of phenyl. Moreover, the peaks of PF_6^- in $PVBVEt(PF_6)_2$

are shown at 832 and 557 cm^{-1}, which are not observed in $PVBVEtBr_2$ and $PVBVEtI_2$, indicating the completely conversion of the anions. The weight-average molar mass M_w of PVBVEtBrCl was obtained by static light scattering. Figure S4 shows the typical static Zimm plot of PVBVEtBrCl in water. The data of static light scattering measurements indicated the M_w of PVBVEtBrCl was 5.49×10^5 g mol^{-1}. X-ray photoelectron spectroscopy (XPS) analysis, scanning electron microscopy (SEM) and the corresponding energy dispersive X-ray (EDX) elemental mapping of $PVBVEt(PF_6)_2$, $PVBVEtBr_2$ and $PVBVEtI_2$ are shown in Figure S5 and S6. The XPS and the corresponding elemental mapping images revealed the presence of C, N, P and F elements in $PVBVEt(PF_6)_2$, C, N and Br in $PVBVEtBr_2$ and C, N, and I elements in $PVBVEtI_2$, which indicate the completely conversion of anionic exchanges in these three ionic polymers.

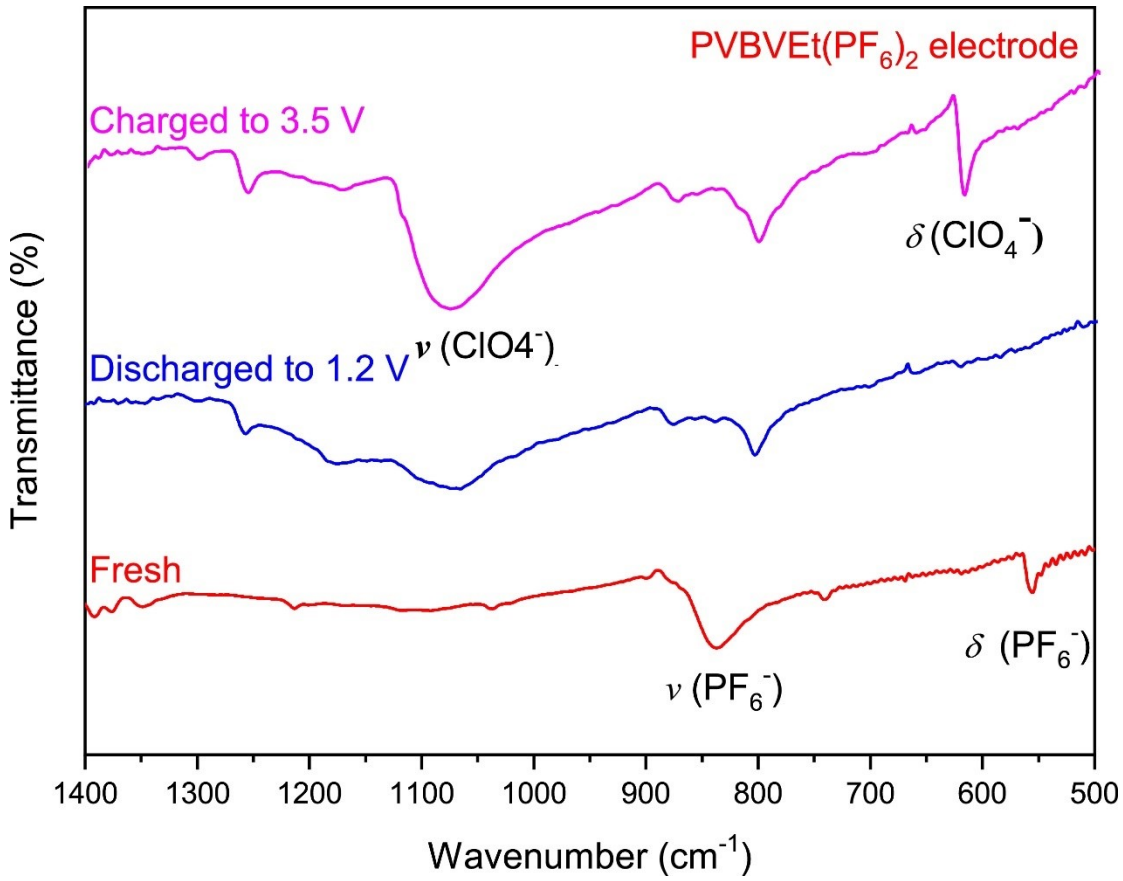

Figure S7. *Ex-suit* FT-IR spectra recorded at different states with a PVBVEt$(PF_6)_2$ as cathode.

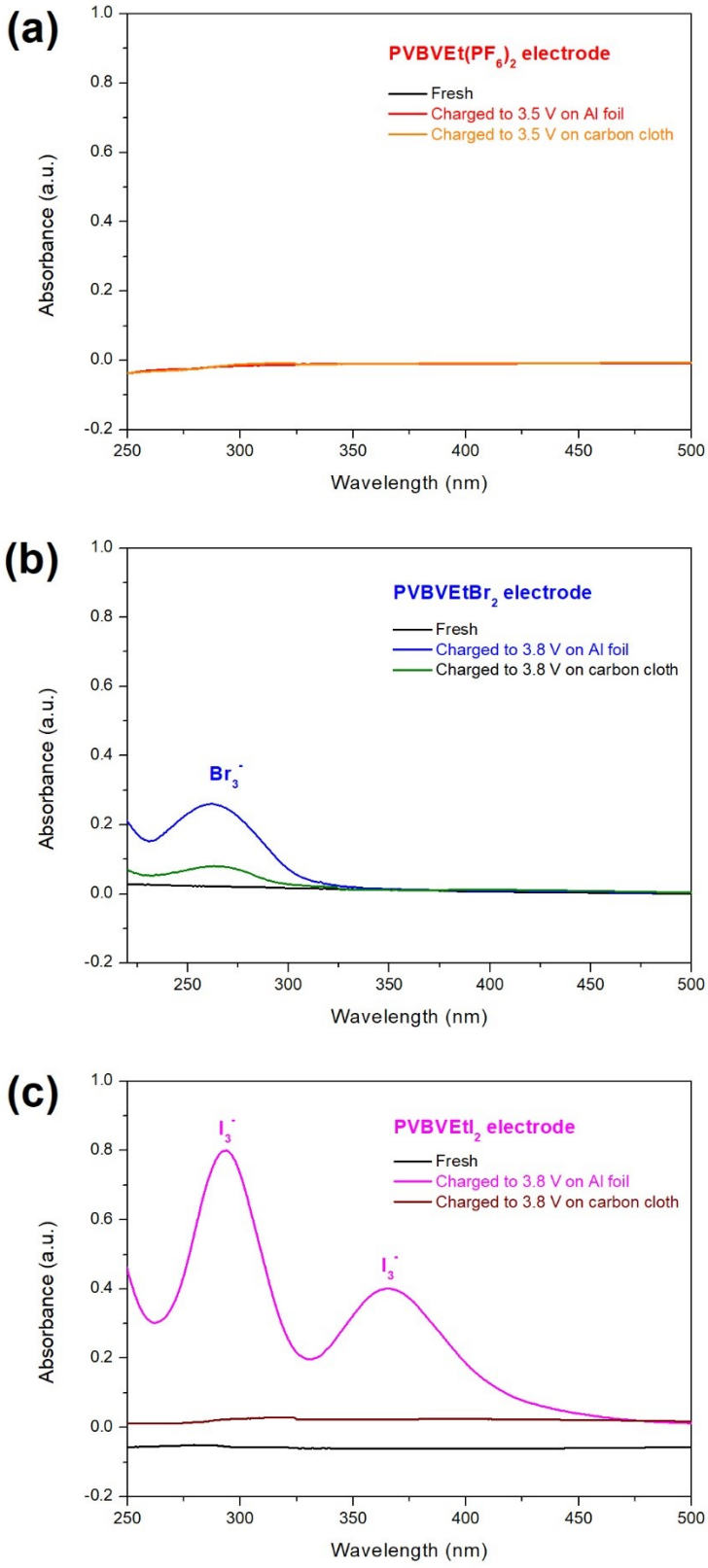

Figure S8. UV/vis spectra of $PVBVEt(PF_6)_2$ (a), $PVBVEtBr_2$ (b) and $PVBVEtI_2$ (c) electrodes on Al foil and carbon cloth at different states immersed in 2M $LiClO_4$/TEGDME electrolytes for 24 h.

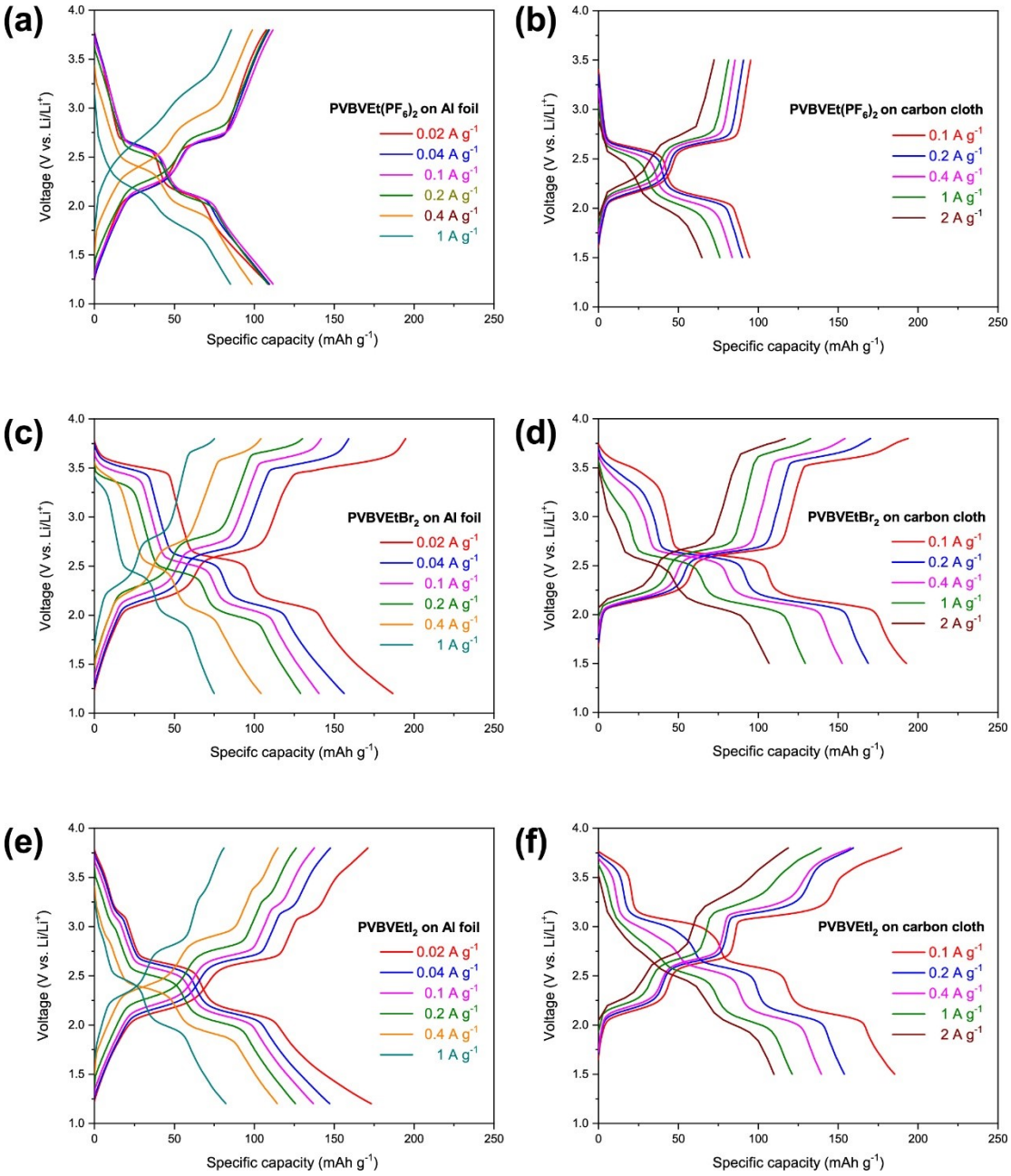

Figure S9. Charge and discharge curves at different current density of $PVBVEt(PF_6)_2$ (a, b), $PVBVEtBr_2$ (c, e) and $PVBVEtI_2$ (e, f) electrodes on Al foil and carbon cloth.

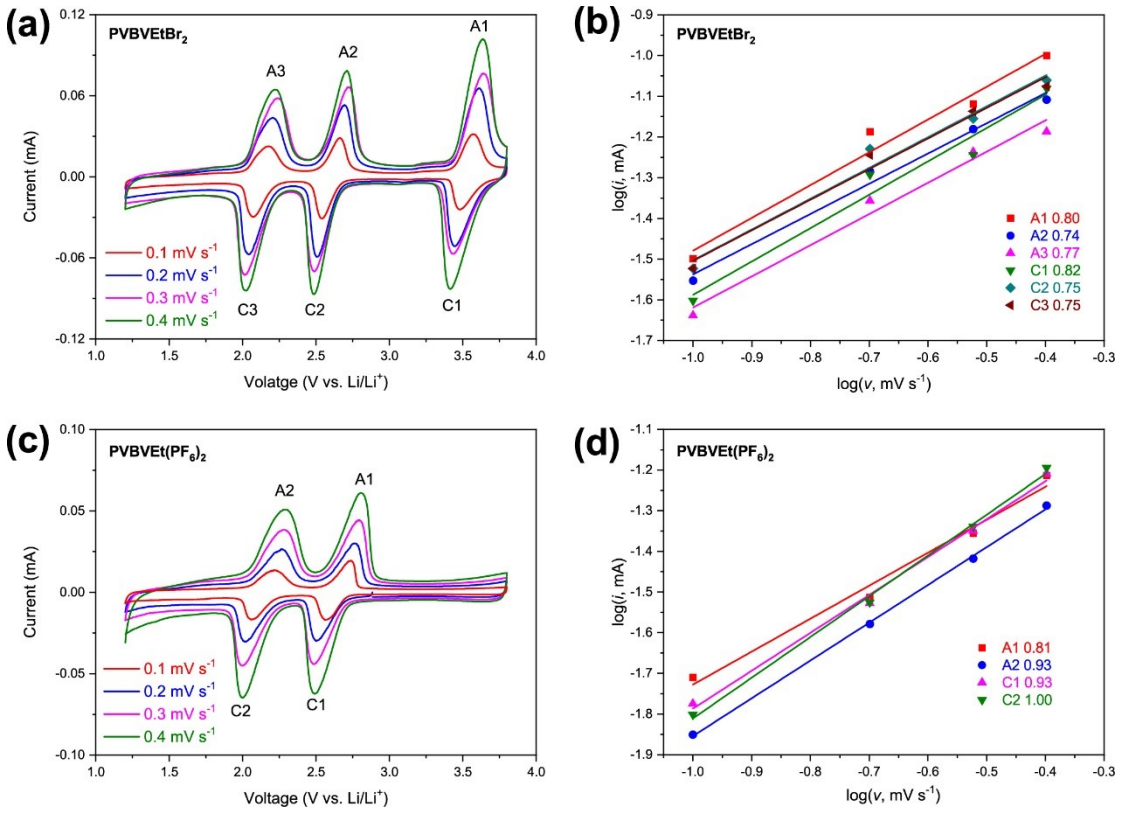

Figure S10. CV profiles of $PVBVEtBr_2$ (a) and $PVBVEt(PF_6)_2$ (c)at different scan rates and the corresponding plots of log(i) versus log(v) at each redox peak (b, d).

The *b*-values for $PVBVEtBr_2$ electrode are calculated to be 0.80,0.74, 0.77 for the anodic reactions and 0.82, 0.75, 0.75 for the cathodic reactions, suggesting a capacitive controlled process. And the b-values of $PVBVEt(PF_6)_2$ electrode are calculated to be 0.81, 0.93 for the anodic reactions and 0.93, 1.00 for the cathodic reactions, indicating the $V^{2+}/V^{\cdot+}$, $V^{\cdot+}/V^{0}$ redox pairs are capacitive controlled process.

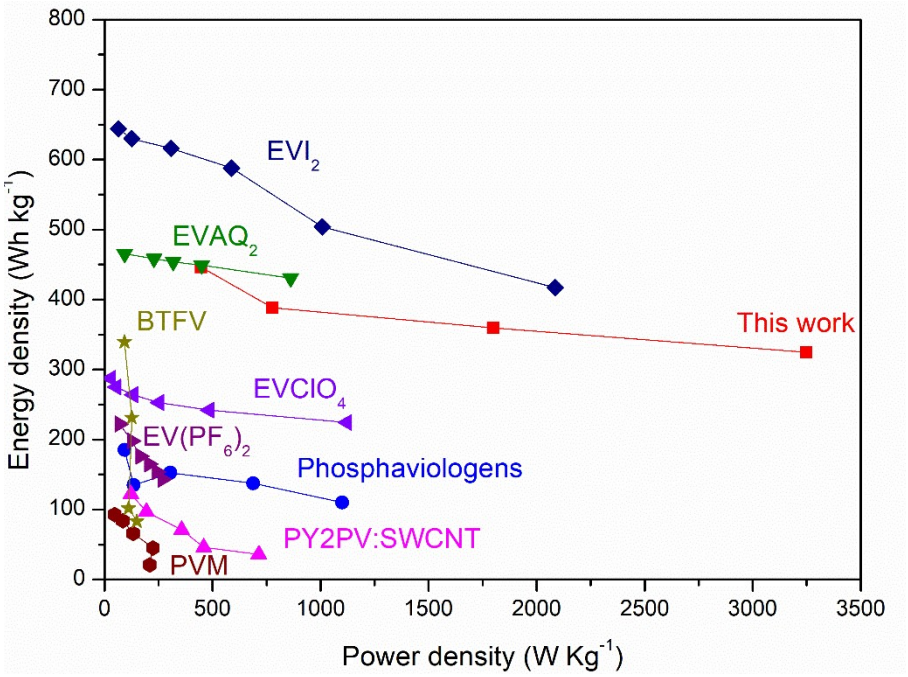

Figure S11. Ragone plot give gravimetric discharge energy density as a function of discharge power density and only viologen-based cathode materials are involved.

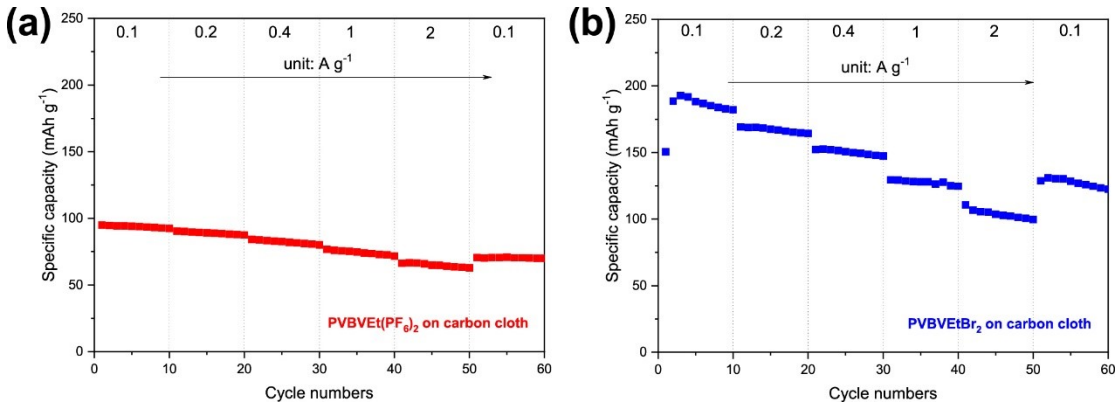

Figure S12. Rate performance of PVBVEt$(PF_6)_2$ and $PVBVEtBr_2$ on carbon cloth.

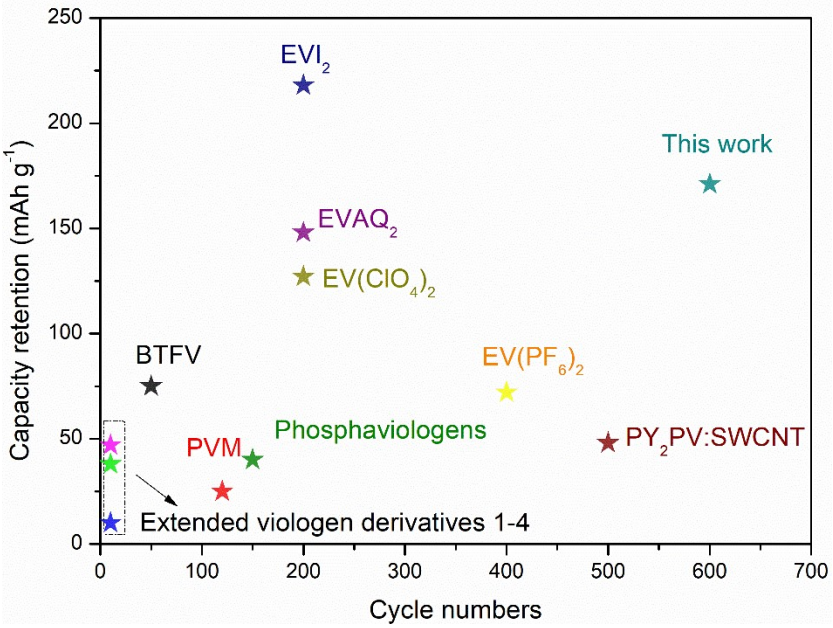

Figure S13. Comparison of the long-term cycling performance of $PVBVEtI_2$/Carbon cloth with that of the previously reported viologens-based cathode materials.

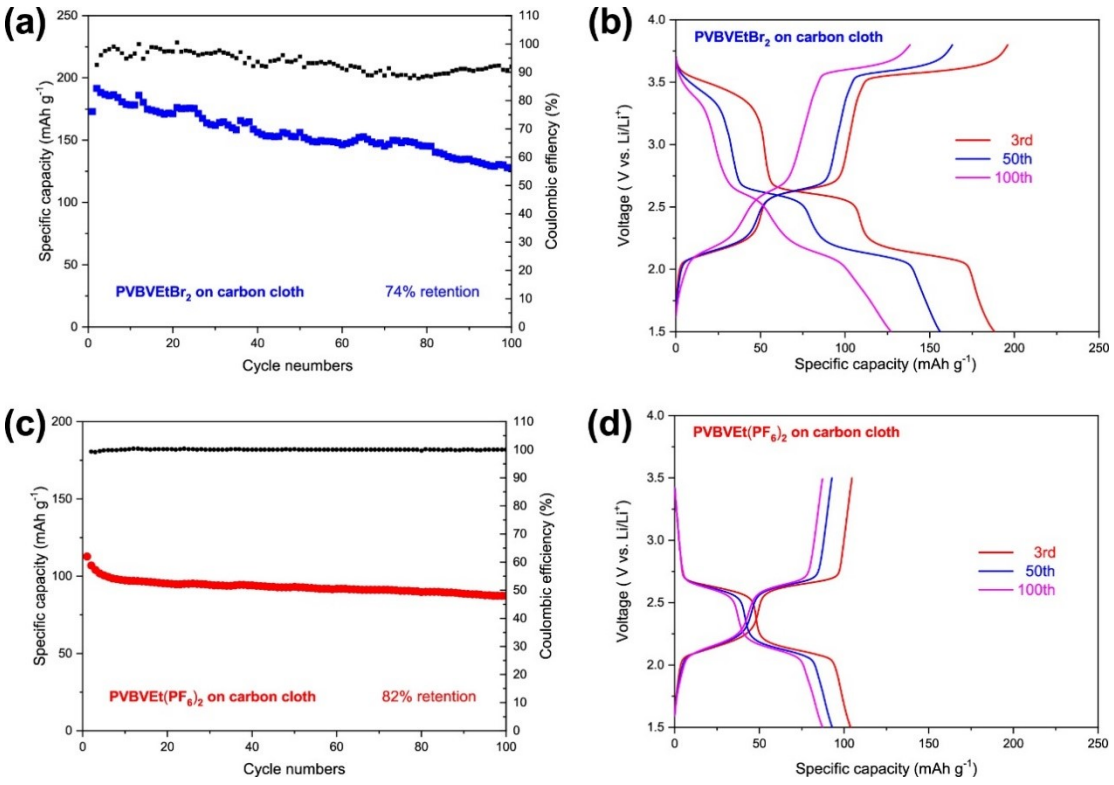

Figure S14. Cycling performance and charge/discharge curves of $PVBVEtBr_2$/carbon cloth (a, b) and $PVBVEt(PF_6)_2$/carbon cloth (c, b) electrodes at the current density of 0.1 A g^{-1}.

Table S1. ESI characteristics of $PVBVEtI_2$ in Al foil and carbon cloth

Electrode materials	R_s (Ω)	R_{ct} (Ω)	n_{dl}	$n_{active\ mass}$	$D_{app}\times10^{-12}$ ($cm^2\ s^{-1}$)	τ_0 (s)
$PVBVEtI_2$/Al	6.72	447.10	0.73	0.60	0.03	177
$PVBVEtI_2$/CC	8.16	94.85	0.84	0.89	0.1	77

where R_s: the equivalent series resistance, R_{ct} :the charge transfer resistance, n_{dl}: an exponent corresponding to the constant phase element representing double-layer capacitance, $n_{active\ mass}$: an exponent corresponding to the constant phase element representing charge storage stemming from the active-mass in the bulk, D_{app}: the apparent diffusion constant (D_{app}) is calculated using the Equation S1, $\tau_{0:}$ the corresponding time constant τ_0 (=1/f_0), f_0 obtained from the Bode plots when θ = −45°.

$$D_{app} = \frac{R^2T^2}{2A^2n^4F^4C^2{\sigma_\omega}^2} \qquad \text{Equation S1}$$

where R is the molar gas constant, T is the absolute temperature, A is the surface area of the electrode material, n is the number of electrons involved in the electrode reaction, F is the Faraday constant, C is the Li concentration within the working electrode and σ_ω is the coefficient of the Warburg element, which is related to the real-part of the impedance according to the Equation S2.

$$Z' = R_s + R_{ct} + \sigma_w\omega^{-1/2} \qquad \text{Equation S2}$$

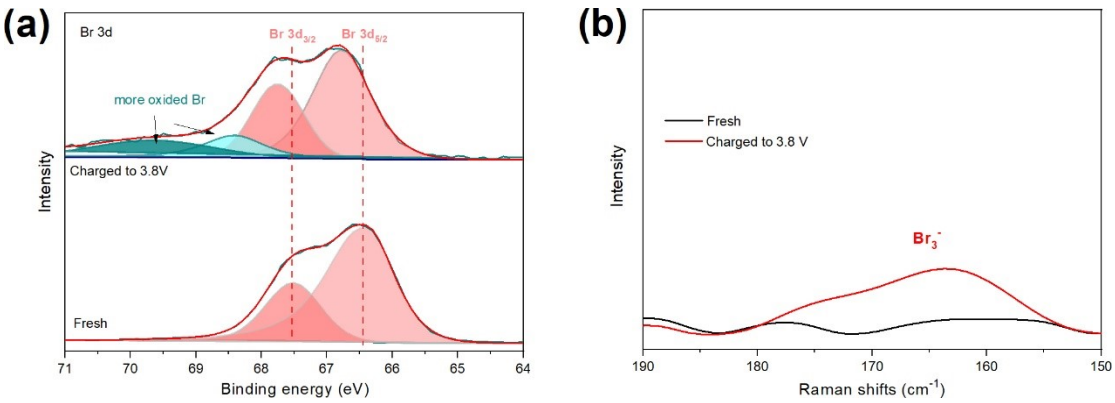

Figure S15. *Ex-situ* XPS (Br 3d) spectra (a) and *ex-situ* Raman spectra (b) of PVBVEtBr$_2$ electrode at fresh state and charged to 3.8 V.

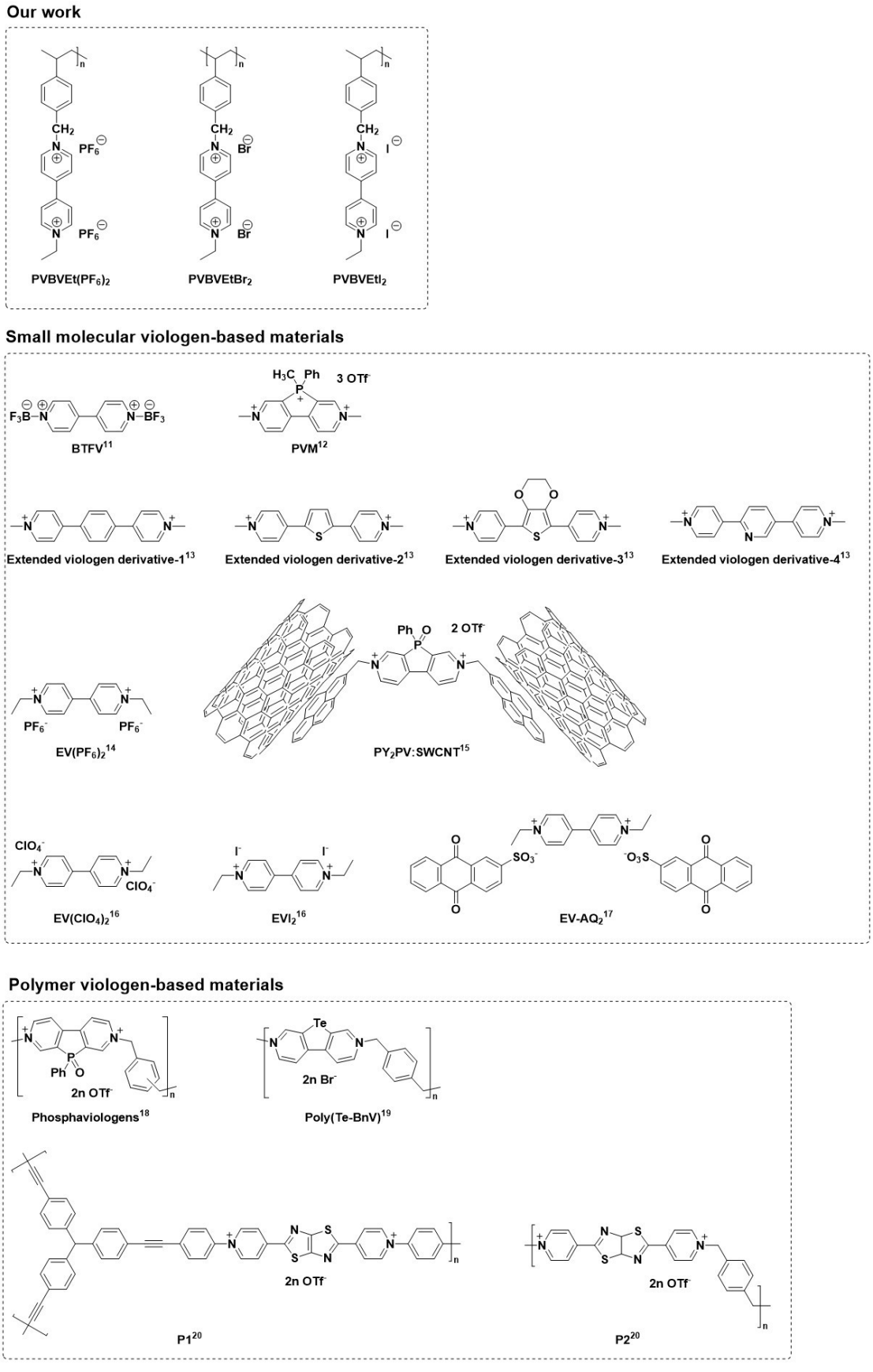

Figure S16. Structure illustration of viologen-based electrode materials for LIBs.

Table S2. The performance comparison of $PVBVEtX_2$, X = PF_6^-, Br^-, and I^- electrode with the reported viologen-based electrodes for LIBs.

Name	Capacity [a]	Voltage plateau (V vs. Li)	Cycling Life [b]	Rate Capability [c]	Ref.
Our work					
$PVBVEt(PF_6)_2$	108 (0.2 C)	2.67/2.15	100/84%	84 (11 C)	
$PVBVEtBr_2$	185 (0.1 C)	3.53/2.67/2.15	100/74%	77 (5 C)	
$PVBVEtI_2$	186 (0.1 C)	3.66/3.12/2.67/2.15	100/71%	85 (5 C)	
$PVBVEtI_2$/Carbon cloth	185 (0.5 C)	3.66/3.12/2.67/2.15	600 (89%)	110 (10 C)	
Small molecular viologen-based electrode materials					
BTFV	175 (0.3 C)	2.15/1.55	50 (~30%)	~50 (1.8 C)	11
PVM	31 (0.5 C)	2–4.5 (no voltage plateau)	120 (~92%)	7 (10 C)	12
Extended viologen derivative-1	70 (0.2 C)	~2	10 (~54%)	/	13
Extended viologen derivative-2	67 (0.2 C)	~2	10 (~15%)	/	13
Extended viologen derivative-3	54 (0.2 C)	~2	10 (~18%)	/	13
Extended viologen derivative-4	65 (0.2 C)	~2	10 (~72%)	/	13
$EV(PF_6)_2$	101 (0.1 mA cm^{-1})	2.4/2.0	400 (80%)	65 (0.6 mA cm^{-1})	14
PY_2PV:SWCNT	48 (1 C)	1.95-3.5	500 (100%)	16 (20 C)	15
$EV(ClO_4)_2$	130 (0.1 C)	2.46/1.94	200 (98%)	102 (5 C)	16
EVI_2	230 (0.1 C)	3.74/3.06/2.41/1.98	200 (96%)	149 (5 C)	16
$EV\text{-}AQ_2$	199.2 (0.1C)	2.53/2.31/2.18	200 (81%)	184 (2 C)	17
Polymer viologen-based electrode materials					
Phosphaviologens	74 (0.5C)	1.8–3.2 (no voltage plateau)	150 (84%)	44 (10 C)	18
Poly(Te-BnV)	684 (0.07 C)	0.001–3 (no voltage plateau)	45 (73%)	252 (2.9 C)	19

P1	554.2 (50 mA g^{-1})	0.005–3 (no voltage plateau)	1000 (100%)	127.4 (1.6 A g^{-1})	20
P2	299.1 (50 mA g^{-1})	0.005–3 (no voltage plateau)	1000 (26%)	~50 (1.6 A g^{-1})	20

[a] the number in the brackets show the current density or C-rate based on the theoretical capacity; [b] the number in the brackets show the capacity retention; [c] the number in the brackets show the current density or C-rate.

NMR spectra

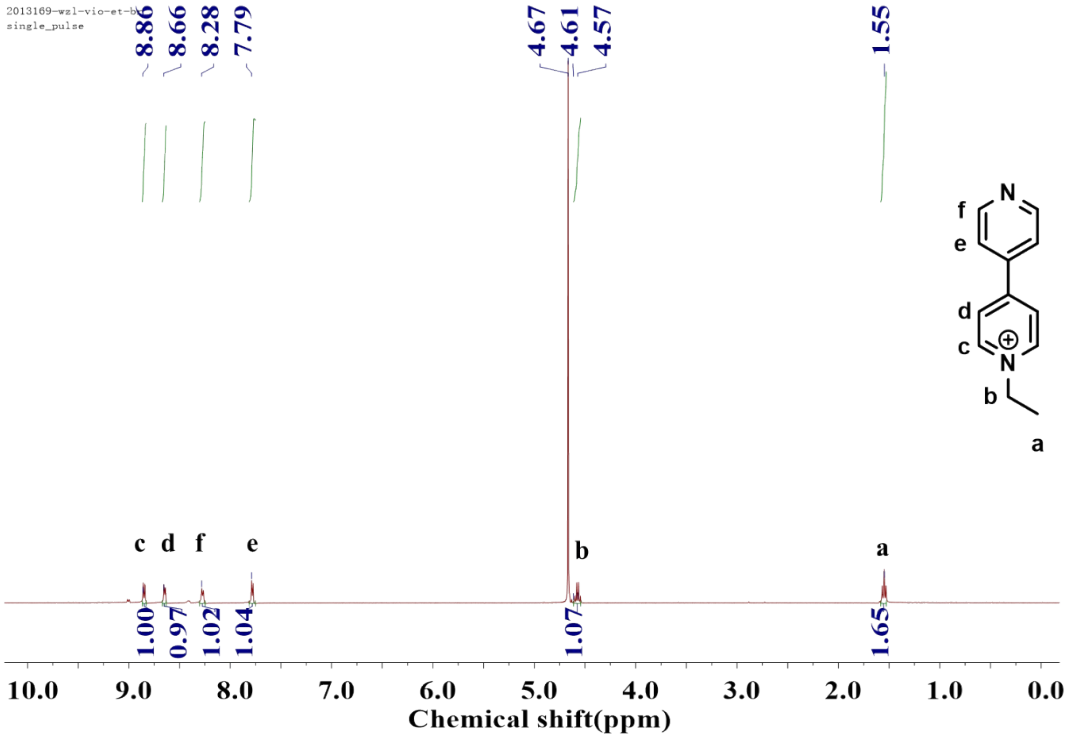

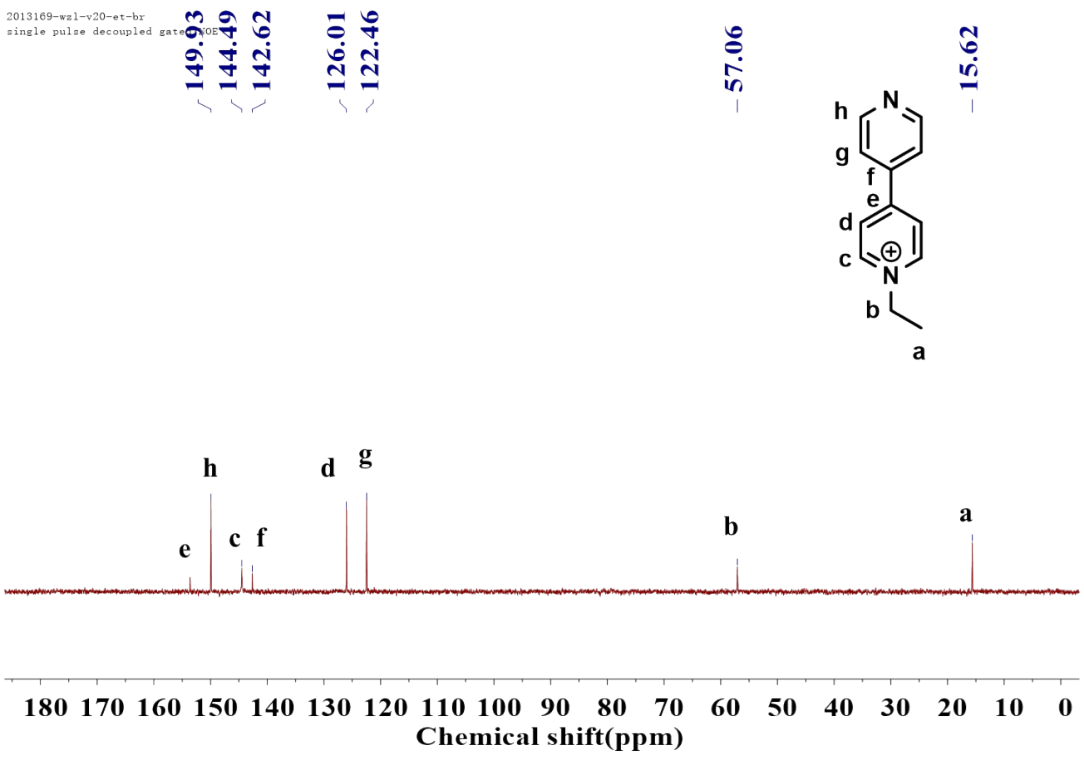

Figure S17. ^{1}H NMR and ^{13}C NMR of EtVBr in D_2O.

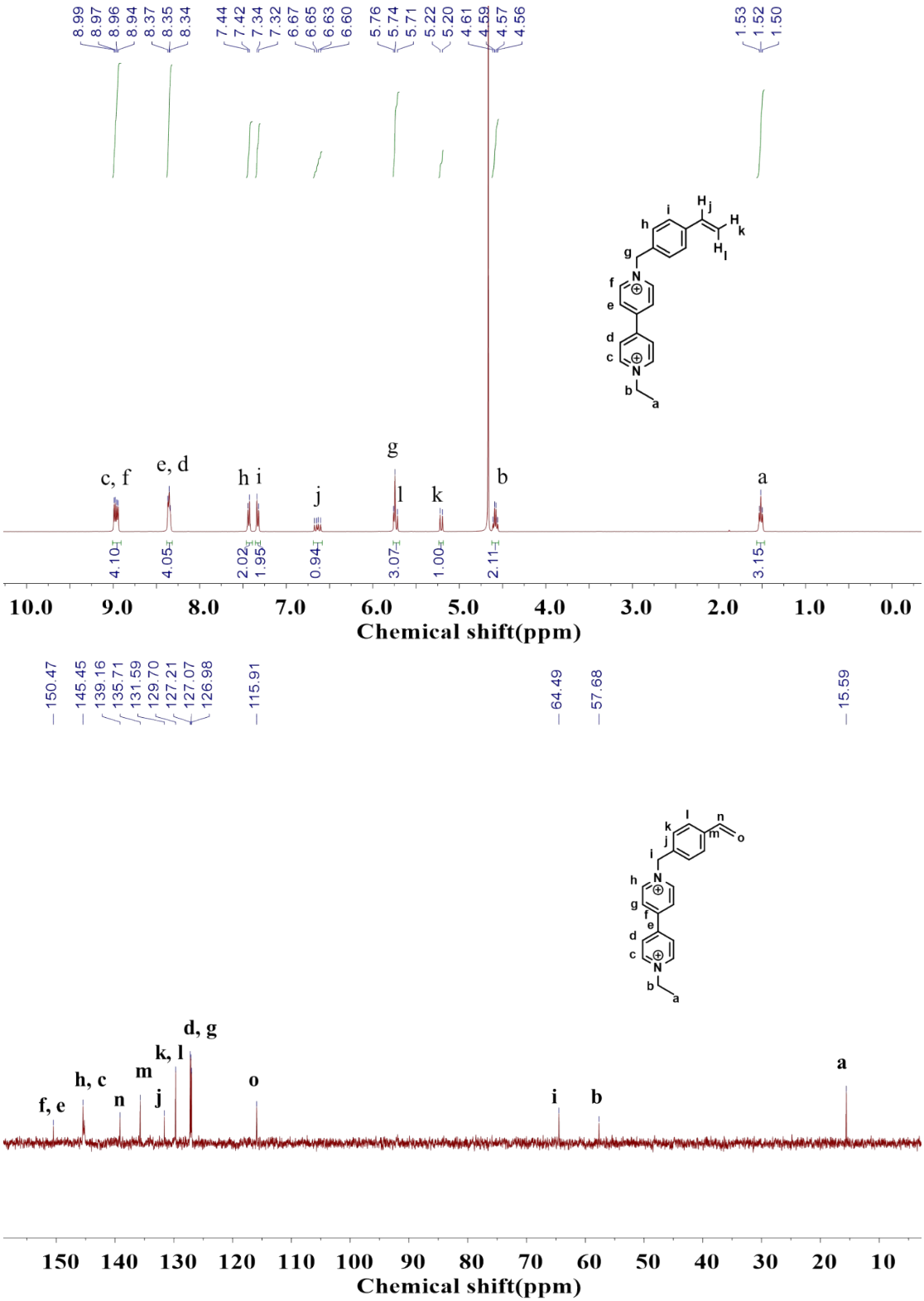

Figure S18. ^{1}H NMR and ^{13}C NMR of VBVEtBrCl in D_2O.

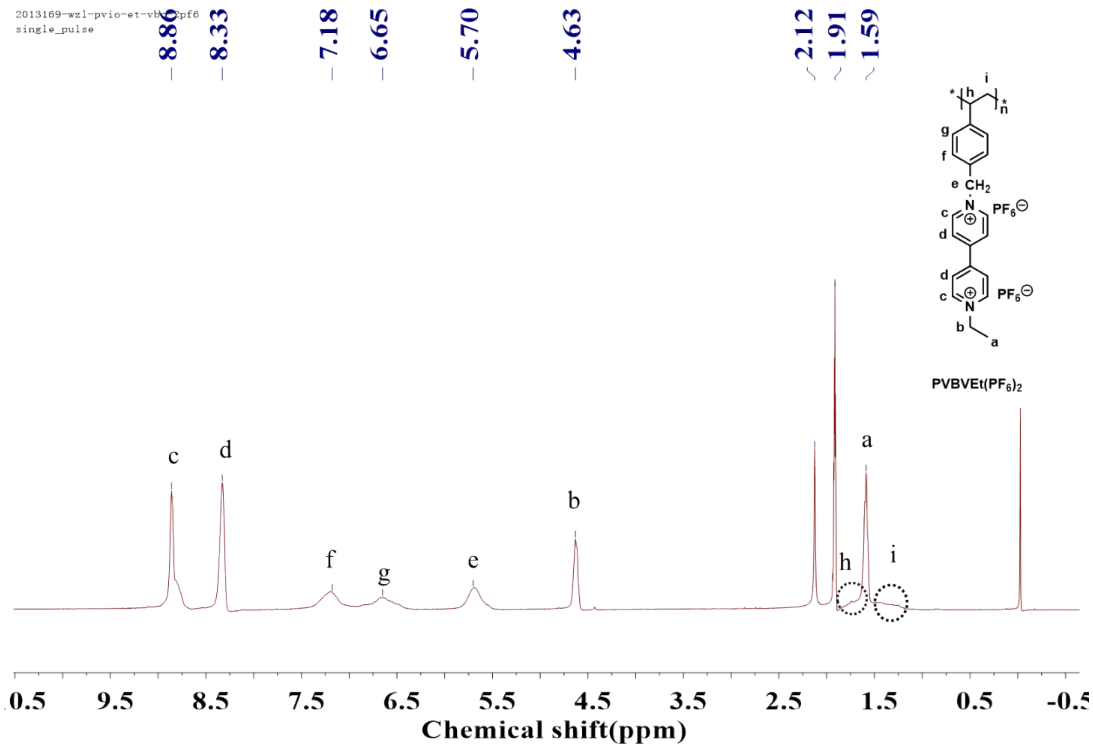

Figure S19. ^{1}H NMR of PVBVEt$(PF_6)_2$ in CD_3CN.

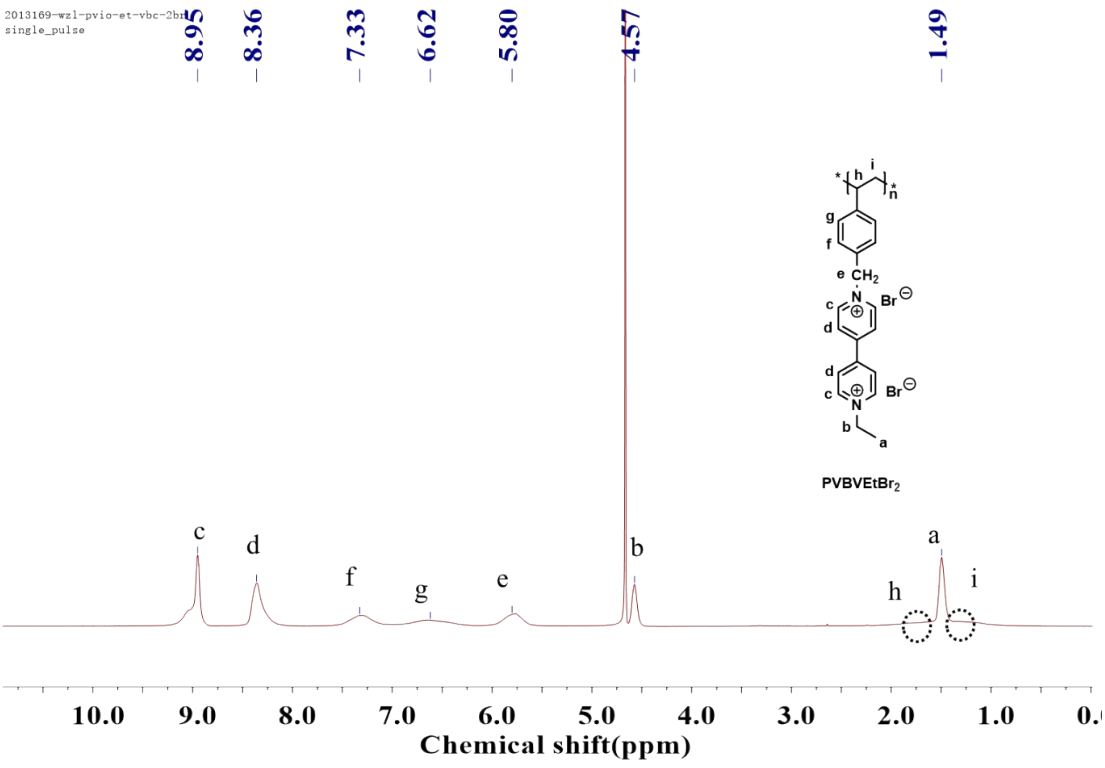

Figure S20. ^{1}H NMR of $PVBVEtBr_2$ in D_2O.

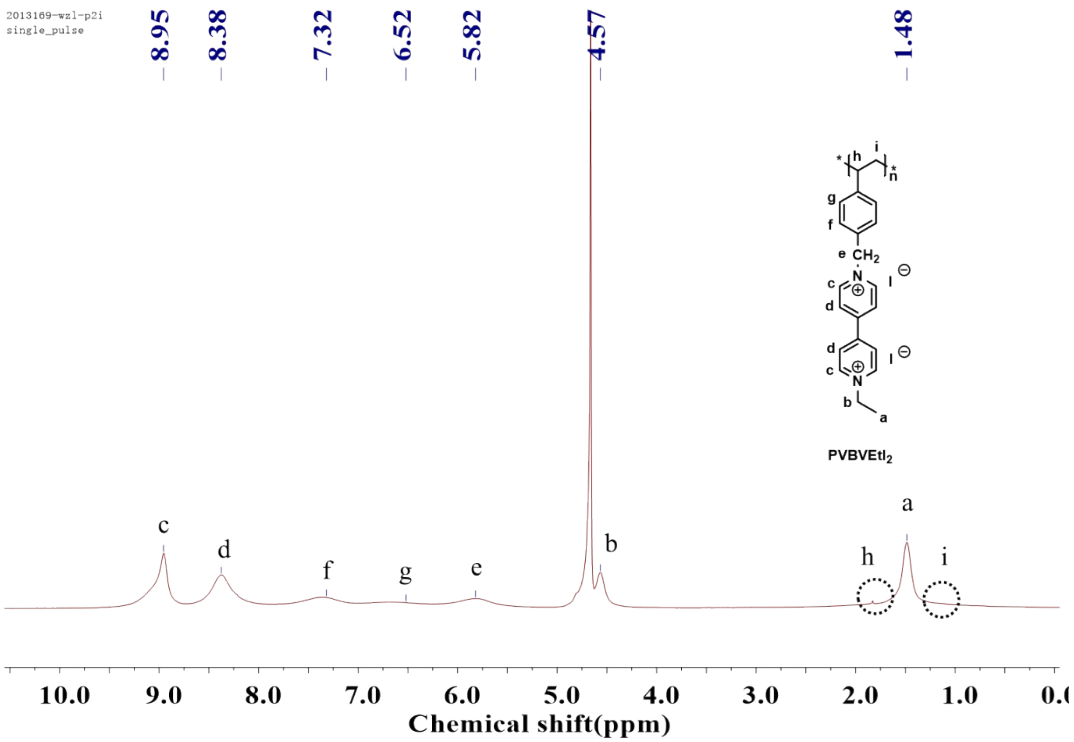

Figure S21. ^{1}H NMR of $PVBVEtI_2$ in D_2O.

Reference

1. S. Suriyakumar, K. Madasamy, M. Kathiresan, M. H. Alkordi and A. M. Stephan, *J. Phys. Chem. C*, 2018, **122**, 27843-27849.
2. J. Li, L. Yang, B. Yuan, G. Li and J. Y. Lee, *Mater. Today Energy*, 2017, **5**, 15-21.
3. A. Natarajan, K. Murugavel, K. Madasamy, S. Suriyakumar, N. Illayaraja, N. Anupriya, M. Christy, K. S. Nahm, Y. Zhou and A. M. Stephan, *Ionics*, 2019, **25**, 3837-3845.
4. Y. Sun, Q. Zou and Y.-C. Lu, Adv. *Energy Mater.*, 2019, **9**, 1903002.
5. A. B. Ikhe, N. Naveen, K.-S. Sohn and M. Pyo, *Electrochim. Acta*, 2018, **283**, 393-400.
6. M. Boota, M. Rajesh and M. Bécuwe, *Mater. Today Energy*, 2020, **18**, 100532.
7. S. Sathyamoorthi, M. Kanagaraj, M. Kathiresan, V. Suryanarayanan and D.

Velayutham, *J. Mater. Chem. A*, 2016, **4**, 4562–4569.

8. C. Chen, S. Zhang, Y. Zhu, Y. Qian, Z. Niu, J. Ye, Y. Zhao and X. Zhang, *RSC Adv.*, 2018, **8**, 18762–18770.
9. B. Hu and T. L. Liu, *J. Energy Chem.*, 2018, **27**, 1326–1332.
10. L. Liu, Y. Yao, Z. Wang and Y.-C. Lu, *Nano Energy*, 2021, **84**, 105897.
11. A. Ghosh and S. Mitra, *RSC Adv.*, 2015, **5**, 105632–105635.
12. C. R. Bridges, A. M. Borys, V. A. Béland, J. R. Gaffen and T. Baumgartner, *Chem. Sci.*, 2020, **11**, 10483–10487.
13. M. Kato, H. Sano, T. Kiyobayashi and M. Yao, *ChemSusChem*, 2020, **13**, 2379–2385.
14. M. Chen, L. Liu, P. Zhang and H. Chen, *RSC Adv.*, 2021, **11**, 24429–24435.
15. C. R. Bridges, M. Stolar and T. Baumgartner, *Batteries Supercaps*, 2020, **3**, 268–274.
16. T. Ma, L. Liu, J. Wang, Y. Lu and J. Chen, *Angew. Chem., Int. Ed.*, 2020, **59**, 11533–11539.
17. Z. Wang, Q. Fan, W. Guo, C. Yang and Y. Fu, *Adv. Sci.* 2021, 9, 2103632.
18. M. Stolar, C. Reus and T. Baumgartner, *Adv. Energy Mater.*, 2016, **6**, 1600944.
19. G. Li, B. Zhang, J. Wang, H. Zhao, W. Ma, L. Xu, W. Zhang, K. Zhou, Y. Du and G. He, *Angew. Chem., Int. Ed.*, 2019, **58**, 8468–8473.
20. L. Chen, X. Zhu, Y. Zhang, G. Gao, W. Xue, S. Zhang, X. Wang, Q. Zhang and X. He, *J. Mater. Chem. A*, 2021, **9**, 18506–18514.